phys. stat. sol. (a) **162**, 421 (1997)

Subject classification: 73.40.Lq; 73.40.Ei; S6

Simulation of SiC High Power Devices

M. Bakowski[1]) (a), U. Gustafsson[1]) (a), and U. Lindefelt[2]) (b)

(a) Industrial Microelectronics Center, P.O. Box 1084, Isafjordsgatan 22, S-164 25 Kista, Sweden

(b) ABB Corporate Research, S-721 78 Västerås, Sweden

(Received January 31, 1997)

The impact of SiC on high power devices and their applications is analysed using simulations in a very wide range of design voltages. First, a detailed presentation of the anisotropic form of the basic equations and of the physical models for 4H-SiC used in the simulations is given. Following that the application ranges of unipolar and bipolar devices in the domains of voltage and frequency are predicted in the case of IGBTs versus MOSFETs and PiN versus Schottky rectifiers based on comparisons of the on-state voltage and of the total losses. The application limit of the MOSFETs compared to IGBTs and of the Schottky rectifiers compared to PiN rectifiers is predicted to be about 4.5 and 2.5 kV, respectively, in the case of the 4H-SiC polytype. The impact of technological limitations of SiC is illustrated by the case of low channel mobility. The merits of SiC as compared to Si are illustrated by the case of a SiC rectifier operating together with a Si IGBT. Dramatically reduced turn-on losses are demonstrated. The superiority of SiC from the point of view of dynamic avalanche is predicted and illustrated. Finally, some novel SiC switch structures are introduced in response to the reliability problems encountered in ordinary trench MOSFETs.

1. Introduction

Silicon carbide presents a great promise in the fields of high temperature, high power and high voltage devices due to its excellent physical and electronic properties [1 to 3]. The high band gap, high critical electric field strength, high thermal conductivity and high saturation velocity of carriers make it an excellent material from the point of view of high power switches and rectifiers for both low and high frequency applications. The road map of the high power devices is about to be redrawn and some of its new characteristics can already be seen evolving in practise. The expectation of a greatly expanded area of unipolar devices compared to silicon [2, 4 to 7] finds more and more justification in experimental results. Several important questions are actualised in this dynamic situation. How do the new silicon carbide alternatives compare with the established silicon alternatives? What are the relative merits of SiC devices compared to Si devices for the same application? What will the new borders between application areas for different devices look like? What is the performance versus cost economy? What types of devices will evolve first due to maturity of the technology and market conditions? What is the best SiC alternative not only with respect to performance but also with respect to the technological feasibility? What is the best device candidate for a given application con-

[1]) tel: +46 87 52 10 00, fax: +46 87 50 54 30, e-mail: mietek.bakowski@imc.kth.se, ulf.gustafsson@imc.kth.se

[2]) tel: +46 21 32 31 77, fax: +46 21 32 32 12, e-mail: ulf.lindefelt@secrc.abb.se

sidering the maturity level of the SiC material and technology, and their impact on the device performance? All those questions are time dependent and will have to be asked and answered over and over again. It is important, in this context, to quantify the improvements made possible by this new material as well as to determine its limitations.

Simultaneously the issues of efficiency and reliability of power systems are becoming increasingly important. This creates a demand for switching devices with ever lower losses and an interest in reducing the number of switching elements in power system and in increasing the operating frequency. An important question from both an application and device development point of view is then that of the relative merits of different switching devices with respect to voltage level and frequency.

The simulation studies presented in this paper focus on some of the above issues. Especially we focus on 4H-SiC unipolar and bipolar devices for the switch-mode dc-to-ac converters using pulse-width modulation (PWM) [8] in the voltage and frequency range of 1 to 20 kV and 1 to 20 kHz, respectively. Before we embark on these questions using device simulation as the only tool, we will present the equations and the physical models used in our simulations.

2. Basic Simulation Equations and Physical Models

2.1 Basic equations for anisotropic semiconductors within the drift–diffusion approximation

In semiconductor simulation programs it is generally assumed that the semiconductor material is isotropic, which is the case for cubic materials such as Si and GaAs. For SiC and for various nitrides, which generally crystallise in structures of symmetry lower than cubic (except for 3C-SiC), anisotropy must in principle be built into the device simulation programs.

The polytype 4H-SiC (like 6H-SiC) is invariant under all operations of the non-symmorphic space group C_{6v}^4. As a consequence (for details, see [9]) the current density relations for electrons (J_n) and holes (J_p) take the form

$$J_n = -qn\mu_n \nabla\varphi_n + qnD_n^T \nabla T\,, \tag{1a}$$

$$J_p = -qp\mu_p \nabla\varphi_p - qpD_p^T \nabla T\,, \tag{1b}$$

where q is the elementary charge, $n\,(p)$ the the electron (hole) density, $\varphi_n\,(\varphi_p)$ the quasi-Fermi potential for electrons (holes), $\mu_n\,(\mu_p)$ the electron (hole) mobility, and nD_n^T (pD_n^T) the Soret coefficient for electrons (holes). Furthermore, both the mobilities and the Soret coefficients are tensors of rank 2. It can be shown [9] that for the hexagonal polytypes of SiC, the 2nd rank transport tensors have the diagonal form

$$\boldsymbol{\sigma} = \begin{pmatrix} \sigma_1 & 0 & 0 \\ 0 & \sigma_1 & 0 \\ 0 & 0 & \sigma_2 \end{pmatrix}, \tag{2}$$

where the symbol $\boldsymbol{\sigma}$ is used to denote any of the transport tensors in (1).

The continuity equations for the flow of electrons and holes maintain their usual form even in anisotropic materials, whereas Poisson's equation for anisotropic materials, determining the electrostatic potential ψ, is given by

$$\nabla(\varepsilon\nabla\psi) = q(n - p - N_D^+ + N_A^-)\,. \tag{3}$$

Here ε is the dielectric tensor and N_{D}^{+} (N_{A}^{-}) is the concentration of ionised donors (acceptors). The dielectric tensor has the same form as the representative tensor $\boldsymbol{\sigma}$ in (2).

In case of non-isothermal modelling the heat conduction equation for anisotropic materials must also be added to the set of semiconductor equations [9 to 11]. However, in this article only isothermal simulations are considered.

A simulation program based on the equations discussed here has been developed together with Technology Modeling Associates Inc. The capability to solve the semiconductor equations for anisotropic materials is available as an Advanced Application Module (AAM) to Medici and Davinci, called the Anisotropic Materials AAM.

2.2 Physical models for 4H-SiC

Since the majority of simulations considered in this article has been performed for 4H-SiC we will confine the presentation to physical models for this polytype only. However, as will be seen, only very few models are directly designed for 4H-SiC. Most of the models for 4H-SiC actually stem from 6H-SiC, and, in some cases, even from Si.

2.2.1 Low-field mobility model

In [12] the results from measurements of electron and hole majority carrier mobilities in both 4H- and 6H-SiC as functions of temperature, doping and direction in epitaxially grown crystals are presented. The results for N-doped (n-type) and Al-doped (p-type) 4H-SiC can be expressed as

$$\mu_{\mathrm{n},\perp} = \mu_{\mathrm{n}}\,, \qquad \mu_{\mathrm{p},\perp} = \mu_{\mathrm{p}}\,, \tag{4a}$$

$$\mu_{\mathrm{n},\parallel} = 1.2\mu_{\mathrm{n}}\,, \qquad \mu_{\mathrm{p},\parallel} = \mu_{\mathrm{p}}\,, \tag{4b}$$

for directions orthogonal ($\perp$) and parallel ($\parallel$) to the hexagonal c-axis. In these expressions the quantity $\mu_{\mathrm{n,p}}$ can for temperatures higher than room temperature approximately be expressed as

$$\mu_{\mathrm{n,p}} = \mu_{\mathrm{n,p}}^{\mathrm{min}} + \frac{\mu_{\mathrm{n,p}}^{\mathrm{delta}}}{1 + \left(\dfrac{N_{\mathrm{D}} + N_{\mathrm{A}}}{N_{\mathrm{n,p}}^{\mu}}\right)^{\gamma_{\mathrm{n,p}}}} \left(\frac{T}{300\ \mathrm{K}}\right)^{\alpha_{\mathrm{n,p}}} \tag{4c}$$

with the parameter values

$$\begin{aligned}
&\mu_{\mathrm{n}}^{\mathrm{min}} = 0\ \mathrm{cm}^2/\mathrm{V\,s}\,, && \mu_{\mathrm{p}}^{\mathrm{min}} = 15.9\ \mathrm{cm}^2/\mathrm{V\,s}\,,\\
&\mu_{\mathrm{n}}^{\mathrm{delta}} = 947\ \mathrm{cm}^2/\mathrm{V\,s}\,, && \mu_{\mathrm{p}}^{\mathrm{delta}} = 108.1\ \mathrm{cm}^2/\mathrm{V\,s}\,,\\
&N_{\mathrm{n}}^{\mu} = 1.94 \times 10^{17}\ \mathrm{cm}^{-3}\,, && N_{\mathrm{p}}^{\mu} = 1.76 \times 10^{19}\ \mathrm{cm}^{-3}\,,\\
&\gamma_{\mathrm{n}} = 0.61\,, && \gamma_{\mathrm{p}} = 0.34\,,\\
&\alpha_{\mathrm{n}} = -2.15\,, && \alpha_{\mathrm{p}} = -2.15\,.
\end{aligned} \tag{4d}$$

Note that this mobility model does not contain the effects of electron–hole scattering, which may be important in power devices operating under high-injection conditions.

2.2.2 Relative dielectric constant

No value for the relative dielectric function for 4H-SiC seems to be published. We therefore use the (low frequency) values for 6H-SiC measured by Patrick and Choyke [13]

$$\varepsilon_{\perp} = 9.66\,, \qquad \varepsilon_{\parallel} = 10.03\,. \tag{5a}$$

In a more recent investigation [14] the following values were obtained:

$$\varepsilon_{\perp} = 9.76\,, \qquad \varepsilon_{\parallel} = 9.98\,. \tag{5b}$$

Since 4H-SiC has somewhat larger band gap than 6H-SiC, one may expect the dielectric constants in 4H-SiC to be somewhat smaller than in 6H-SiC.

2.2.3 Impact ionisation

No detailed model parameters describing impact ionisation in 4H-SiC have been reported. However, relatively detailed measurements of impact ionisation have been performed for 6H-SiC [1, 15, 16]. We have assumed that 4H-SiC is not too different from 6H-SiC in this respect. This may be a reasonable assumption around room temperature where impact ionisation $\parallel c$ in 6H-SiC is mainly caused by holes [1, 15]. If this is the case also in 4H-SiC, then because of the strong similarities in valence band structures between these two polytypes [17], they may have very similar impact ionisation properties. At higher temperature, however, also electrons start to contribute to impact ionisation [1], and since 4H- and 6H-SiC have quite different conduction band structures [17] there are reasons to speculate on different high-temperature behaviour of the impact ionisation for the two polytypes.

The total electron–hole impact ionisation rate is expressed as

$$G_{\mathrm{II}} = \frac{1}{q}\left(|\alpha_{\mathrm{n}} J_{\mathrm{n}}| + |\alpha_{\mathrm{p}} J_{\mathrm{p}}|\right), \tag{6}$$

where α_{n} and α_{p} are both diagonal tensors with diagonal elements $\alpha_{\mathrm{n}\parallel}$, $\alpha_{\mathrm{n}\perp}$ and $\alpha_{\mathrm{p}\parallel}$, $\alpha_{\mathrm{p}\perp}$, respectively. The tensor components are then modelled by

$$\alpha_{\mathrm{n}\parallel} = \alpha_{\mathrm{n}}\,, \qquad \alpha_{\mathrm{p}\parallel} = \alpha_{\mathrm{p}}\,, \tag{7a}$$

$$\alpha_{\mathrm{n}\perp} = \alpha_{\mathrm{p}}/3.5\,, \qquad \alpha_{\mathrm{p}\perp} = \alpha_{\mathrm{p}}\,, \tag{7b}$$

where

$$\alpha_{\mathrm{n,p}}(E) = a_{\mathrm{n,p}} \exp\left(-\frac{b_{\mathrm{n,p}}}{E_J}\right). \tag{8}$$

Here E_J is the projection of the electric field in the direction of the current, i.e., $E_J = \mathbf{E}\cdot\mathbf{J}/|\mathbf{J}|$. By fitting to the results in [1] and [15], the parameters a_{n} and b_{n} can be expressed as (with T in K)

$$a_{\mathrm{n}}(T) = 7.628\times10^{6}(T/300)^{2} + 1.506\times10^{6}(T/300) - 4.184\times10^{6}\ [\mathrm{cm}^{-1}]\,, \tag{9a}$$

$$b_{\mathrm{n}}(T) = 2.58\times10^{6} \quad \text{(independent of } T\text{)} \qquad [\mathrm{V/cm}]\,, \tag{9b}$$

$$a_{\mathrm{p}}(T) = 1.469\times10^{6}(T/300)^{2} - 1.083\times10^{7}(T/300) + 3.1\times10^{7}\ [\mathrm{cm}^{-1}]\,, \tag{9c}$$

$$b_{\mathrm{p}}(T) = 1.90\times10^{7} \quad \text{(independent of } T\text{)} \qquad [\mathrm{V/cm}]\,. \tag{9d}$$

2.2.4 Intrinsic band gap and band gap narrowing

According to [18] (p. 31), the band gap for 4H-SiC at $T \approx 4.2$ K is E_g (4.2 K) = 3.285 eV. This value is based on two components: a measured exciton band gap E_{gx} = 3.265 eV, and a measured exciton binding energy $E_x \approx 0.020$ eV, i.e., $E_g = E_{gx} + E_x$. To our knowledge, the temperature derivative of the band gap in 4H-SiC has not been published. Again we will borrow the value obtained for 6H-SiC, namely ([19], or see [20] for the original work)

$$\mathrm{d}E_g/\mathrm{d}T = -3.3 \times 10^{-3}\ \mathrm{eV/K}\,; \qquad 300\ \mathrm{K} \le T \le 700\ \mathrm{K}\,. \tag{10}$$

Assuming the same temperature dependence all the way down to 4 K (which may thus not be correct according to (10)), one gets the approximate model

$$E_g(T) = 3.19 - 3.3 \times 10^{-3}(T - 300\ \mathrm{K})\ \mathrm{eV}\,. \tag{11}$$

Another model for E_g (T) is obtained by using instead the low-temperature band gap obtained in [21], namely E_g ($T \approx 50$ K) = 3.41 eV. Note that this value is substantially larger than the value E_g (4.2 K) = 3.285 eV quoted above.

There seems to exist no model for doping-induced band gap narrowing for any polytype of SiC today. Thus, lacking a model, we simply use the Slotboom formula with parameters for Si (see [22], p. 37). A theoretical model for band gap narrowing is at present being worked out, however [23].

2.2.5 Effective masses

A model for the intrinsic number requires both electron and hole density-of-states effective masses. These can be obtained from recent band structure calculations. It was found in [24] that the conduction band minimum in 4H-SiC is at the M-point in the Brillouin zone, thus giving rise to three equivalent conduction band minima. The calculated effective mass components in the principal directions are [24] (in units of the free electron mass)

$$m_c(\mathrm{M\Gamma}) = 0.57\,, \qquad m_c(\mathrm{MK}) = 0.28\,, \qquad m_c(\mathrm{ML}) = 0.31\,, \tag{12}$$

which also compares very well with recent cyclotron resonance measurements [25]. In (12) the ML direction corresponds to electron motion along the hexagonal c-axis, while the directions MΓ and MK correspond to electron motion in a plane perpendicular to the c-axis. This leads to an electron density-of-states effective mass $m_{de} = (3^2 \cdot 0.57 \cdot 0.28 \cdot 0.31)^{1/3} = 0.76$ (free electron masses).

The top of the valence bands consists of three separate bands, v1, v2 and v3 [24]. In the immediate vicinity of the valence band maximum the surfaces of constant energy are well approximated by ellipsoids. Using the results in [24], it is found that the uppermost valence band (v1) has a density-of-states effective mass $m_{dv1} = (0.61 \cdot 0.61 \cdot 1.62)^{1/3} = 0.84$. Similarly, the second band (v2), which is 0.009 eV below the first band due to spin–orbit interaction ($\Delta_{so} \approx 9.4$ meV), has a density-of-states effective mass $m_{dv2} = 0.79$, whereas the third band (v3), 73 meV below the first band due to crystal-field interaction, has a density-of-states effective mass $m_{dv3} = 0.78$. The density-of-states effective mass m_{dv} for the top of the valence bands, i.e., including the combined effect of all three valence bands, then becomes (in units of

the free electron mass)

$$m_{\mathrm{dv}}(T) = \left[0.84^{3/2} + 0.79^{3/2}\ \exp\left(-\frac{0.009}{k_{\mathrm{B}}T}\right) + 0.78^{3/2}\ \exp\left(-\frac{0.073}{k_{\mathrm{B}}T}\right)\right]^{2/3}, \quad (13)$$

where k_{B} is the Boltzmann constant. At room temperature, for instance, $m_{\mathrm{dv}}(300\ \mathrm{K}) \approx 1.20$. Note that the temperature dependence in the hole density-of-states effective mass displayed in (13) is not complete since the effective mass components $m_{\mathrm{v}1}$ etc., obtained from band structure calculations, are only valid at $T = 0$ K. Using (11) and (13) one gets for the intrinsic number $n_{\mathrm{i}}\ (300\ \mathrm{K}) = 5.27 \times 10^{-8}\ \mathrm{cm}^{-3}$.

2.2.6 Donors and acceptors

The most common dopant for producing n-type SiC is N. Doping with N leads to a donor (substituting on C-site) which has two different energy levels below the conduction band. The reason for the two ionisation energies is that in 4H-SiC there are two inequivalent C (or Si) sites, one with cubic (k) surrounding and the other with hexagonal (h) surrounding [26]. Nitrogen atoms substituting on these sites therefore experience somewhat different surroundings, giving rise to different ionisation energies. In fact, it was found in [26] that k-type N causes deeper levels than h-type N. It is also expected that the number of k-type and h-type donors are more or less the same.

In 4H-SiC the two ionisation energies are [18, 27]

$$E_{\mathrm{c}} - E_{\mathrm{h}} = 52.1\ \mathrm{meV}\,, \qquad E_{\mathrm{c}} \text{ - } E_{\mathrm{k}} = 91.8\ \mathrm{meV}\,, \quad (14)$$

where E_{c} denotes the conduction band minimum and E_{h} (E_{k}) the ground state energy level of the hexagonal (cubic) N donor. Note that the relatively large binding energies lead to incomplete ionisation.

If one is not concerned with the dynamic effects of incomplete ionisation, these two donor levels can be lumped together and replaced by a single effective level E_{d} at

$$E_{\mathrm{c}} - E_{\mathrm{d}} = 65\ \mathrm{meV} \quad (15)$$

with a degeneracy factor $g_{\mathrm{d}} = 2$. This result can be obtained by requiring

$$\frac{0.5N_{\mathrm{D}}}{1 + g_{\mathrm{d}}\ \dfrac{n}{N_{\mathrm{c}}}\ \exp\left(\dfrac{E_{\mathrm{c}} - E_{\mathrm{h}}}{k_{\mathrm{B}}T}\right)} + \frac{0.5N_{\mathrm{D}}}{1 + g_{\mathrm{d}}\ \dfrac{n}{N_{\mathrm{c}}}\ \exp\left(\dfrac{E_{\mathrm{c}} - E_{\mathrm{k}}}{k_{\mathrm{B}}T}\right)} = \frac{N_{\mathrm{D}}}{1 + g_{\mathrm{d}}\ \dfrac{n}{N_{\mathrm{c}}}\ \exp\left(\dfrac{E_{\mathrm{c}} - E_{\mathrm{d}}}{k_{\mathrm{B}}T}\right)} \quad (16)$$

at $T = 300$ K. Here N_{c} is the effective density-of-states for electrons and N_{D} is the concentration of N atoms. The right-hand side of (16) represents the number of ionised donors for the single effective donor level, while the left-hand side represents the actual number of (incompletely) ionised N donors. It has been assumed that the number of k-type donors is the same as the number of h-type donors and that, for simplicity, both electron and hole density-of-states effective masses are equal to the free electron mass. Equation (16) can only be satisfied for an effective ionisation energy $E_{\mathrm{c}} - E_{\mathrm{d}}$ that depends on both electron density and temperature. With a single constant value $E_{\mathrm{c}} - E_{\mathrm{d}}$

= 65 meV it is possible, however, to closely mimic the electron density dependence of the left-hand side of (16) for $T = 300$ K.

It should be noted that there is some uncertainty whether the values in (14) are correct. According to [18] (p. 88), other results have been obtained, for instance the pairs of binding energies (66 meV, 124 meV) [26] and (45 meV, 100 meV) [27].

To produce p-type SiC, doping can be done with Al, Ga or B. Of these acceptors, Al (substituting on Si site) is the shallowest with [18]

$$E_a - E_v \approx 0.191 \text{ eV}, \tag{17}$$

where E_v is the energy at the top of the valence band, E_a is the ground state energy of the Al acceptor, and a degeneracy factor $g_a = 4$ is assumed. As in the case of donors, also acceptors should in principle show two different energy levels corresponding to the two inequivalent sites. However, this energy difference seems to be too small in Al-doped 4H-SiC to be readily detectable.

2.2.7 Shockley-Read-Hall (SRH) and Auger recombination

At present time not much has been published about energy levels, concentrations and capture cross-sections for recombination centres in SiC. In simulations it is therefore customary to assume that the effect of recombination centres can be described by the conventional one-level SRH recombination/generation formula (see for instance [22] (p. 105)) in which the trap level is put in the middle of the band gap and the electron and hole minority carrier lifetimes are treated as adjustable parameters.

The parameters describing the Auger recombination rate (see for instance [22] (p. 109)) are, to our knowledge, unknown for any SiC polytype. We have therefore used the parameter values valid for Si [28].

3. Devices for High Power Applications

The main issues to be treated below are those of the on-state losses, switching losses (turn-on and turn-off losses) and basic technology and material limitations for both well established and novel device concepts applied to SiC. The impact of the technology and material limitations is reflected in the choice and description of the simulated structures. All the device structures must be realised using chemical vapour deposition (CVD) epitaxy, reactive ion etching (RIE) and relatively shallow ion implantations. All the deep drive-in diffusions are excluded. The state of the art of oxide and gate technologies is considered by the choice of realistic channel mobility values. The material limitations are accounted for by the choice of realistic lifetime values. In the low frequency range the on-state voltage becomes the most important parameter while the total losses have to be considered in the medium and high frequency range. The basic limitation of all bipolar power switches is the dynamic avalanche. This material limitation is expected to be much less severe in SiC compared to Si as will be illustrated in the case of the PiN diode.

The models for SiC are still very limited and often inaccurate. The necessary condition for considering the results justified is that the questions asked do not go beyond the scope of the existing models. The completeness and accuracy of the models is by necessity tied to the maturity of the material and device technologies and can only be im-

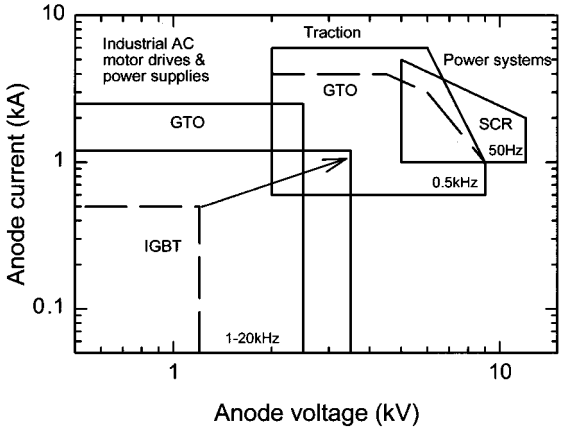

Fig. 1. The application areas of the high power devices

proved with time. We find the current models adequate for the questions we address in this work. Also, since our predictions are of comparative nature the absolute accuracy is not critical.

Application areas of high power devices together with the type of the devices used are shown in Fig. 1. The picture is today dominated entirely by silicon devices. The situation for 1992 is shown by the dashed lines [29]. The most dramatic development during the last five years and in the years to come is in the area of Insulated Gate Bipolar Transistors (IGBTs). Both IGBT and Gate Turn-Off (GTO) devices require an antiparallel diode of matching voltage blocking capability. The silicon bipolar power devices have reached the limit given by the material itself in the form of the dynamic avalanche limit. This applies to PiN diodes [30], IGBTs [31, 32] and GTOs [33] but is especially acute in the case of PiN rectifiers since it often sets the limit on how fast the IGBTs can be operated. Another area is that of dc voltage reliability and cosmic radiation induced failures which came recently into focus [34]. This forces silicon device manufacturers to reduce the electric field in the devices by new designs or increased margins to the critical electric field strength [35], which often leads to increased losses. Silicon carbide presents a promising alternative with respect to both dynamic avalanche and cosmic radiation [36] due to the one order of magnitude higher critical electric field strength. This will be illustrated below in the case of the antiparallel PiN diode with respect to dynamic avalanche.

The main division in power devices is that between unipolar and bipolar devices. The voltage range of unipolar devices is expected to be greatly expanded with advent of SiC power switches and rectifiers. The most striking development in SiC devices right now is in the field of Schottky rectifiers [37 to 41]. In the following sections we will determine the potential application range of PiN versus Schottky power rectifiers and MOSFET versus IGBT power switches based on an analysis of the total losses in the domains of voltage and frequency.

3.1 Unipolar versus bipolar devices. 4H- versus 6H-SiC

In this section the performance of the SiC trench gate MOSFETs and IGBTs is analysed with respect to the design voltage and frequency. The simulation set-up is identical to

that in [42] with the same conservative gate driving conditions given by $R_{on} = 10\ \Omega$ and $R_{off} = 50\ \Omega$. The gate voltage is switched between 15 and −15 V. The total losses are calculated for a 2 kA switching device (either MOSFET or IGBT) in a dc-to-ac PWM converter as described in the same reference. All the simulated structures have the same basic cell structure. The cell pitch is equal to 48 μm, mesa width W equals 9 μm and trench width G equals 39 μm. The bulk mobility values are used for the channel mobility in order to simplify the assumptions made. In [43] the influence of the non punch-through (NPT) and punch-through (PT) designs, carrier lifetime and temperature on the conduction properties of the 4.5 and 10 kV 6H-SiC IGBTs has been investigated. The NPT structures were found superior to the PT structures due to wider temperature range of normal operation and a positive temperature coefficient of the on-state voltage. As a result of that investigation all the IGBT devices in the present paper are of the NPT type. All the MOSFET devices are designed with rectangular field distribution and are of the PT type. The main difference between the MOSFETs and IGBTs is a p^+ substrate in the case of the IGBTs instead of the n^+ doped substrate in the case of MOSFETs. The only parameter adjusted when varying the design voltage is the width and doping of the drift region. The optimum value of the diode lifetime was found to be between 0.2 and 0.5 μs depending slightly on the design voltage. In the presented material, the value of 0.5 μs is used for all diodes. The optimum lifetime value for the IGBTs was found to be between 0.5 and 2 μs depending slightly on the design voltage and the polytype. In the presented material, the value of 2 μs is used for all IGBTs. The lifetime in the MOSFETs was set to 0.5 μs. The simulated structure and the simulation circuit are shown as insets in Fig. 2a and b, respectively. All the simulations were performed at 473 K.

In Figs. 2a and b the total losses for 4.5 kV MOSFETs and IGBTs are shown as functions of frequency for 4H- and 6H-SiC, respectively, at two current densities of 20 and 100 A/cm^2. The anode voltage is half of the design voltage. The specific on-resistance of the 4H- and 6H-SiC MOSFETs is 38 and 345 mΩ cm^2, respectively. The

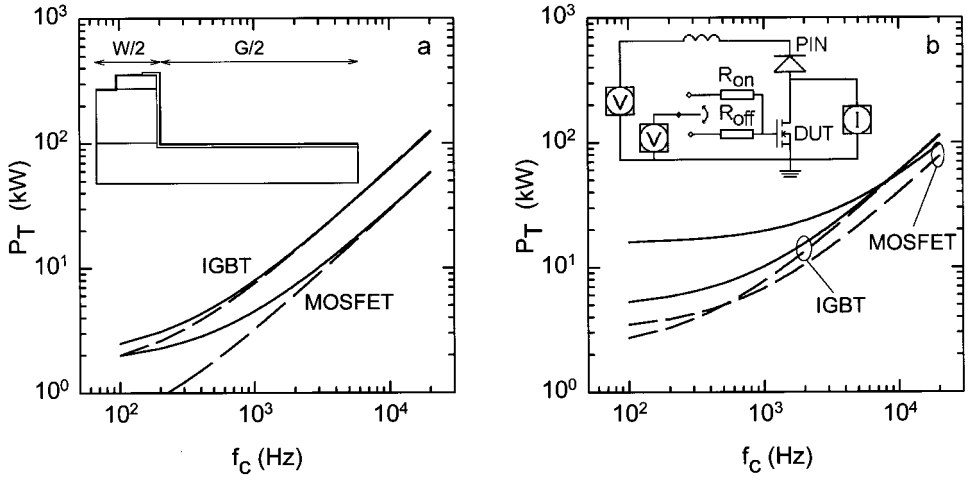

Fig. 2. a) The total losses for 4.5 kV 4H-SiC MOSFET and IGBT and b) the total losses for 4.5 kV 6H-SiC MOSFET and IGBT. The cross-section of the device structure (half cell) and simulation set-up are shown in the insets

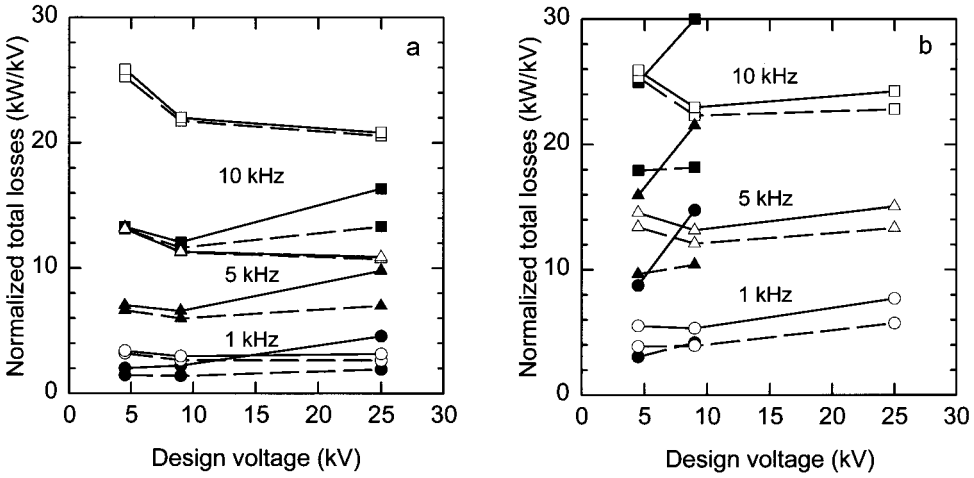

Fig. 3. a) The total losses normalised by design voltage for 4H-SiC MOSFETs (solid symbols) and IGBTs (empty symbols) at commutation frequencies 1 kHz (circles), 5 kHz (triangles) and 10 kHz (squares) and at current densities 20 A/cm^2 (dashed lines) and 100 A/cm^2 (solid lines) and b) the total losses normalised by design voltage for 6H-SiC MOSFETs (solid symbols) and IGBTs (empty symbols) at commutation frequencies 1 kHz (circles), 5 kHz (triangles) and 10 kHz (squares) and at current densities of 20 A/cm^2 (dashed lines) and 100 A/cm^2 (solid lines)

on-state voltage of the 4H- and 6H-SiC IGBTs at 100 A/cm^2 is 4.5 and 14.5 V, respectively. In Figs. 3a and b a comparison of total losses normalised by design voltage for MOSFETs and IGBTs in the voltage range up to 25 kV is shown. The superiority of the 4H polytype for both MOSFETs and IGBTs is clearly demonstrated. The difference in total losses between 4H- and 6H-SiC is dramatic in the case of MOSFETs in the whole range of investigated voltages and frequencies. In the case of the IGBTs the difference in total losses between 4H- and 6H-SiC is much less pronounced and becomes significant at frequencies below 2 kHz and at voltages above 10 kV. The difference in on-state voltage is significant in the whole investigated range of voltages also for IGBTs as illustrated by the 4.5 kV values above. The difference between the 4H- and 6H-SiC is even more clear when comparing the total losses between MOSFETs and IGBTs in the same polytype. In 4H-SiC we predict lower total losses for MOSFET devices for all the voltages up to 10 kV at a frequency of 1 kHz and in the whole investigated range of voltages at frequencies above 5 kHz up to a current density of 100 A/cm^2. While in the 6H-SiC case the total losses for MOSFET devices are predicted to be lower only for voltages below 4.5 kV and at frequencies above 10 kHz at 100 A/cm^2.

The on-state voltages for the 4H-SiC devices from Fig. 3a are shown in Fig. 4. It can be seen that the on-state voltage is lower for MOSFETs compared to IGBTs up to about 6 and 4.5 kV at current densities 50 and 100 A/cm^2, respectively.

The calculated on-state voltage values and total losses are somewhat optimistic in the case of MOSFETs since the choice of the PT structure assumes an ideal junction termination for those devices. The data represent thus the best case situation from the point of view of the MOSFETs. Refer to [42] for the illustration of the influence of the drift region width on the total losses of the 4.5 kV MOSFETs. From now on all the presented results are for the 4H-SiC devices.

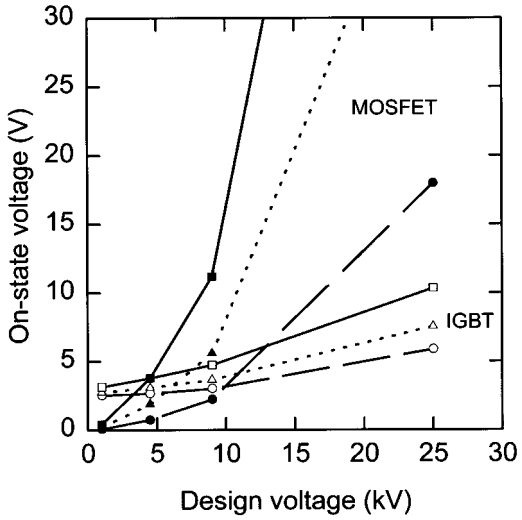

Fig. 4. The on-state voltages for 4H-SiC MOSFETs (solid symbols) and IGBTs (empty symbols) from Fig. 3a at current densities of 20 (dashed line), 50 (dotted line) and 100 A/cm^2 (solid line) as a function of design voltage

3.2 Technology limitations. The case of the 4.5 kV 4H-SiC MOSFET and IGBT

One of the acknowledged areas where SiC technology is not quite mature is that of the gate dielectric. The properties of the SiC/SiO_2 system and those of the SiO_2 gate dielectric are still not satisfactory with respect to the quality of the interface and of the oxide itself. This leads to reduced values of channel mobility and reliability problems [7, 44, 45].

The effect of reduced channel mobility on the electrical characteristics of both MOSFET and IGBT has been investigated. The voltage level chosen for the comparison is 4.5 kV at which both MOSFET and IGBT should have comparable on-state voltage drop. The structure of the devices under investigation is modified as well as the measurement conditions compared to the earlier section. The simulated structures have cell pitch equal to 24 μm and trench width $G = 4$ μm. Both IGBT and MOSFET have the NPT design with respect to the drift region width. This means a drift region doping and width of 2×10^{15} cm^{-3} and 50 μm, respectively. The p-base doping and width are 5×10^{17} cm^{-3} and 2 μm, respectively. The simulation set-up is still the same but the gate resistance is reduced to $R_{on} = 2\ \Omega$ and $R_{off} = 10\ \Omega$. The on-state voltages and the switching losses for the 4.5 kV MOSFET and IGBT are shown in Figs. 5a and b, respectively, for different values of the channel mobility. The channel mobility value of 130 cm^2/Vs corresponds to the bulk mobility value for electrons in the p-base at a temperature of 473 K, according to the mobility model (4c). Some important observations can be made. One is that the on-state voltage of the IGBT is more sensitive to the channel mobility value than the on-state voltage of the MOSFET. This is due to the fact that the on-state voltage of the MOSFET is determined to a larger extent by the resistivity of the n$^-$ (drift) region than the on-state voltage of the IGBT by the voltage drop over the conductivity modulated n$^-$ (base) region. The second is a strong effect of the channel mobility on the turn-on losses and a relative insensitivity of the turn-off losses to the channel mobility for both MOSFET and IGBT. Finally, note that influence of the channel mobility on the on-state voltage and switching losses of both MOSFET and IGBT becomes significantly weaker at channel mobility values larger than about

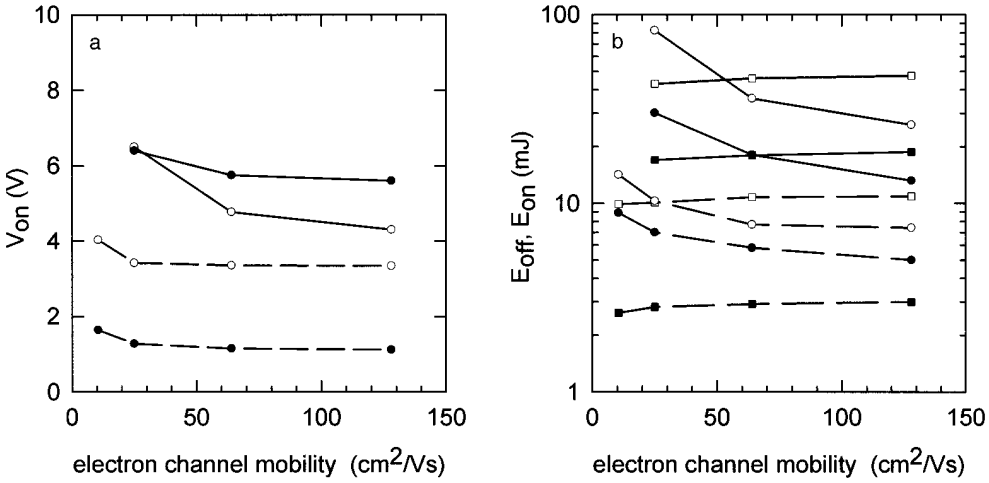

Fig. 5. a) The on-state voltage of the 4.5 kV MOSFET (solid symbols) and IGBT (empty symbols) (see also Fig. 6), at current densities 20 A/cm^2 (dashed lines) and 100 A/cm^2 (solid lines) and b) the turn-on (circles) and turn-off (squares) energy per pulse of the same MOSFET (solid symbols) and IGBT (empty symbols) at current densities 20 A/cm^2 (dashed lines) and 100 A/cm^2 (solid lines). The saturation current density for channel mobility of 10 cm^2/Vs is about 60 A/cm^2 with gate voltage 15 V

60 cm^2/Vs (160 cm^2/Vs at room temperature from (4c)). In Figs. 6a and b the total losses for the 4.5 kV MOSFET and IGBT are plotted as a function of frequency at two current densities, 20 and 100 A/cm^2, and for different values of channel mobility. The total losses are calculated for a 2 kA device (MOSFET and IGBT) in a dc to ac PWM converter, as before. The effect of reduced channel mobility on the total losses becomes

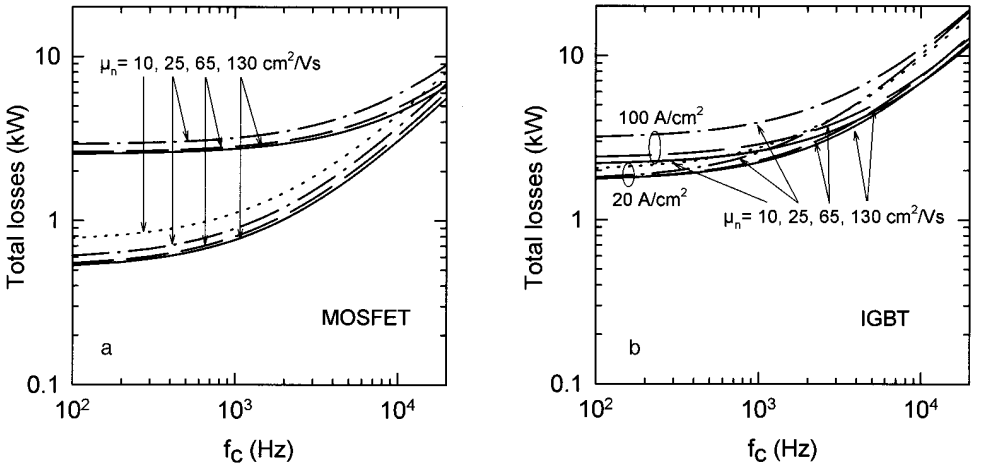

Fig. 6. a) The total losses of the 4.5 kV MOSFET for the channel mobility values of 10, 25, 65 and 130 cm^2/Vs, as indicated in the figure, and at current densities of 20 (lower curves) and 100 A/cm^2 (upper curves) and b) the total losses of the 4.5 kV IGBT for the channel mobility values of 10, 25, 65 and 130 cm^2/Vs and at current densities 20 and 100 A/cm^2, as indicated in the figure

significant first below a value in the range 30 to 60 cm^2/Vs at 473 K. Note the relatively stronger deterioration of the performance in the case of the IGBT compared to the MOSFET.

The channel mobility issue does not appear to be a critical one. A rather moderate channel mobility of about 50 cm^2/Vs at 473 K (130 cm^2/Vs at room temperature) seems to be satisfactory. A room temperature channel mobility value of about 20 cm^2/Vs was for some time reported as the state of the art value for 4H-SiC [46]. Recently a room temperature mobility value of about 70 cm^2/Vs has been reported [47] and it is reasonable to expect further improvements in the future following the increased understanding of the specific nature of the SiO_2/SiC interface [48, 49]. The impact of reduced channel mobility is expected to be more severe at low design voltages [7, 50] where the contribution of the channel resistivity to the total on-resistance is larger. However, as was shown in [51], the 1 kV 4H-SiC MOSFETs are still superior to Si MOSFETs even at the very low channel mobility of less than 15 cm^2/Vs at 373 K. The really critical issues appear to be the ones of charge trapping and reliability.

4. SiC PiN Rectifier with Si IGBT

The SiC devices can find an early application in replacing the Si antiparallel diode working together with a Si switch. Si diodes in this applications are subject to stresses being at the limit of the material properties of Si [30]. There are two benefits to be gained from replacing the Si PiN diode by a SiC PiN rectifier. One is the reduction of losses due to much lower recovery charge of the SiC rectifier and the second is the possibility of much faster operation (higher di/dt) without encountering the limit of dynamic avalanche. Higher di/dt means in turn even further reduction of losses and possible increase in operation frequency. The frequency limit will then be given by the gate controlled switch and the nature of the load.

In Fig. 7 the turn-on waveforms of the 2.5 kV Si IGBT with a Si antiparallel diode and with the Si diode exchanged by a 2.5 kV PiN SiC rectifier are shown under identi-

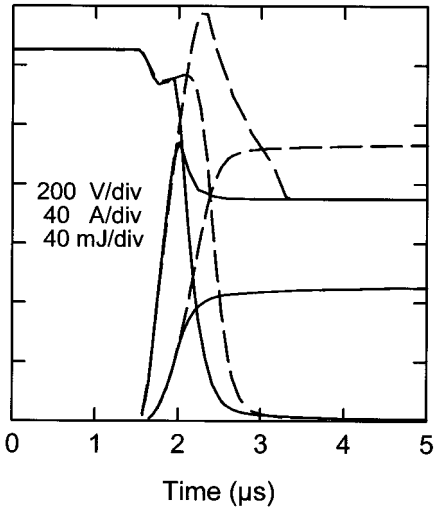

Fig. 7. The simulated current and voltage waveforms at turn-on of the 2.5 kV Si IGBT with Si (dashed lines) and SiC (solid lines) PiN antiparallel diode. The turn-on losses are also shown

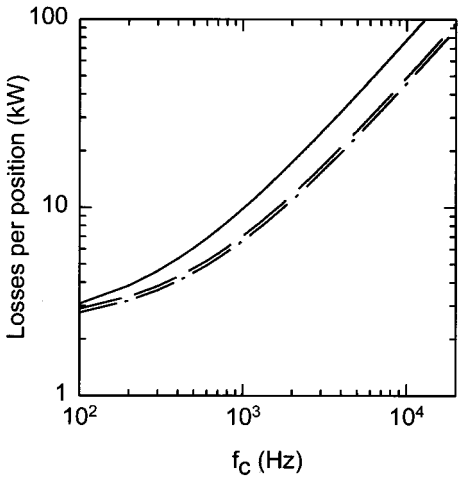

Fig. 8. The total losses for the 2.5 kV Si IGBT with Si PiN (solid line), SiC PiN (dashed line) and SiC Schottky (dash-dotted line) rectifiers at 373 K. The calculated losses are a sum of the IGBT and antiparallel diode losses

cal conditions at 373 K. The simulation set-up is shown as an inset in Fig. 9. Note the large reduction in recovery charge of the diode and in the turn-on losses of the IGBT. The description of the Si devices was calibrated against the measured on-state characteristics and following this an excellent agreement was obtained between measured and simulated turn-on and turn-off waveforms. The total switching losses of the IGBT can be reduced by about 30 % by replacing the Si PiN diode by a SiC PiN rectifier. At the same time the turn-off losses of the SiC PiN rectifier are only about 5% of the turn-off losses of the Si PiN diode. Further improvements can be achieved using a Schottky rectifier. However, the additional gain is not significant as can be seen in Fig. 8 where total losses for a 2 kA Si IGBT operated together with an antiparallel Si PiN, SiC PiN and SiC Schottky rectifier, respectively, in a dc-to-ac PWM converter are compared as a function of frequency. The Schottky barrier height of 1.0 eV was assumed.

The on-state voltage of the SiC Schottky rectifier at 473 K becomes equal to that of the SiC PiN rectifier for design voltages of 2.5 and 3.0 kV using NPT and PT drift region design, respectively. Considering the high temperature and voltage sensitivity of the leakage current characteristic of the Schottky rectifier and expected higher degree of difficulty in realising an effective junction termination, we regard 2.5 kV as the ultimate limit for the SiC Schottky rectifier.

5. Dynamic Avalanche

In Fig. 9 the anode current waveforms at turn-on of the same 2.5 kV IGBT as in Fig. 7 are shown with both Si and SiC diodes but with reduced cathode inductance, $L_k = 1$ nH, and gate resistance, $R_{on} = 2\ \Omega$. The di/dt is now about 5 kA/μs. The influence of the cathode leak inductance on the turn-on losses and on di/dt over the diode is shown in Fig. 10. The simulations in Fig. 9 are performed both with the avalanche model activated (solid lines), which is the standard procedure, and with the avalanche multiplication model excluded (dashed lines). Comparing the current waveforms an evidence of a significant dynamic avalanche effect is clearly seen in the Si diode while the same effect is not present in the SiC diode. Inspection of the internal solutions confirms this observation. This means that the SiC diode operation is more reliable under the same condi-

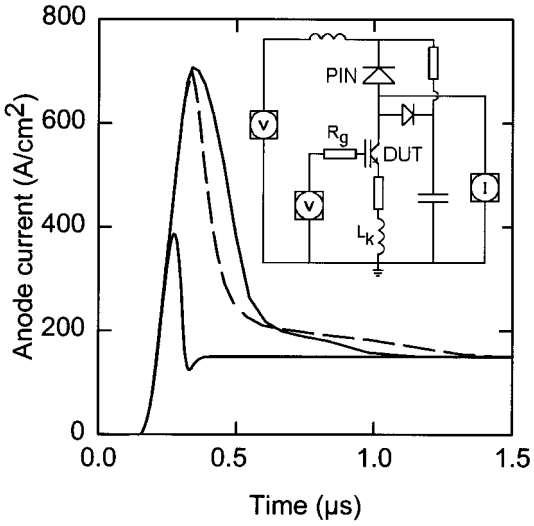

Fig. 9. The simulated current waveforms during turn-on of the 2.5 kV Si IGBT of Fig. 7 operated with Si and SiC PiN rectifiers. Simulations are done with (solid lines) and without (dashed lines) the avalanche multiplication model. The $\mathrm{d}i/\mathrm{d}t$ is about 5 kA/μs

tions and moreover that we can operate the diode faster assuming the IGBT can be turned on faster.

The critical hole current density corresponding to the onset of the dynamic avalanche phenomenon is shown in Fig. 11 for both Si and SiC. The critical hole current density has been calculated using (18) for Si [52]

$$V_{\mathrm{B}} = 5.34 \times 10^{13} N_{\mathrm{D}}^{-3/4}, \tag{18}$$

and (19), based on data in Fig. 4 of [53], for SiC

$$V_{\mathrm{B}} = 3.086 \times 10^{14} N_{\mathrm{D}}^{-0.7097} \tag{19}$$

by substituting an effective doping, $N_{\mathrm{eff}} = N_{\mathrm{D}} + j_{\mathrm{p}}/qv_{\mathrm{sat}}$, for the fixed doping N_{D} in both equations and with v_{sat} values of 1×10^7 and 2×10^7 cm/s for Si and SiC, respec-

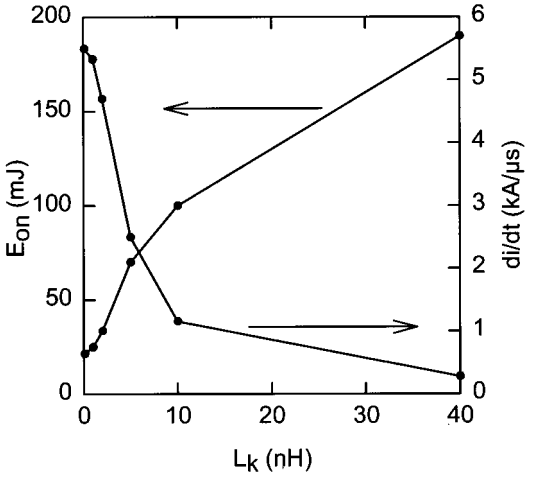

Fig. 10. The influence of the cathode leak inductance on the $\mathrm{d}i/\mathrm{d}t$ and on the turn-on losses

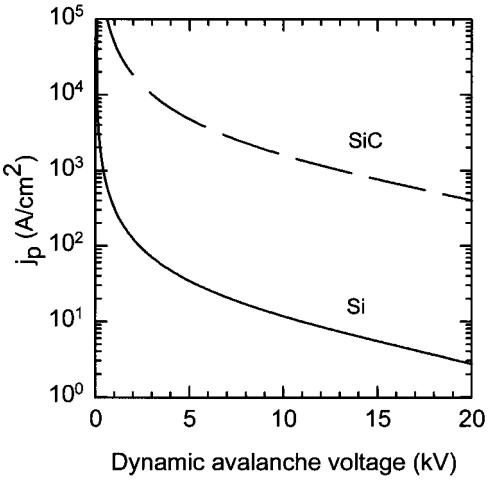

Fig. 11. The critical density of the hole current corresponding to the onset of the dynamic avalanche for the Si (solid line) and SiC (dashed line)

tively. The fixed doping has been set low enough not to limit the voltage range shown and was 1×10^{12} and 1×10^{14} cm^{-3} for Si and SiC, respectively.

The calculated critical hole current density corresponds to homogeneous current distribution. This means that dynamic avalanche can occur at significantly lower current density levels than shown when the current distribution is not homogeneous [33]. This is a typical situation in the bipolar junction transistor (BJT) and GTO. The current distribution in IGBTs is as a rule much more homogeneous due to the influence of the channel resistivity acting as a resistive emitter ballast. Dynamic avalanche phenomena are not necessarily destructive. They are destructive only if enough energy is dissipated into heat so that the temperature increases beyond a certain critical value which makes the phenomenon regenerative by a coupling and mutual reinforcement of thermally generated and avalanche generated carriers leading to a thermal run-away. Another destructive case is when the excess carriers generated by the dynamic avalanche process trigger a latch-up mechanism leading to destruction. In this case an excessive heat generation is not required prior to entering the final destructive phase [33].

SiC is expected to have extremely good dynamic avalanche tolerance due to its basic material properties like high critical field strength, large band gap and good thermal conductivity.

6. Emerging Switching Devices

The basic device concepts of interest for SiC switches are all well known from Si. At present the choice of device concept may have to be made more on the basis of the feasibility or maturity of basic technologies rather than on the basis of desired performance. MOSFETs are an obvious choice. They suffer, however, from the immaturity of the oxide and gate dielectric technology in general. Also the high electric fields in the case of SiC, one order of magnitude higher compared to Si, make the demands set on the MOSFET gate difficult to meet as long as there are no mature alternatives to SiO_2. This is especially true in the case of the trench MOSFETs where high electric field in

the trench corner area is the main reason for instability and premature failure [44]. In this situation the concepts not requiring gate dielectric like static induction transistor (SIT) [54], junction gate field effect transistor (JFET) [55] and [56] and Schottky barrier gate field effect transistor (MESFET) [57] are explored anew. Unfortunately, devices utilising an insulating gate control are preferred from the application point of view due to the simplicity of the gate drive and ease of realisation of normally-off type of devices. As a remedy to this the cascode solutions involving MOSFET as the emitter control element similar to the proposed earlier in Si like the BJT-MOS cascode (so called emitter-open turn-off) and the GTO-MOS cascode could be employed. One example is the hybrid solution consisting of a Si power MOSFET connected in series with the source region of a SiC power MESFET or JFET [58].

At the same time a new family of devices is being actualised by the necessity to reduce the extremely high electric field in the gate region. One way of doing that is by utilising a buried grid concept. In Figs. 12a and b the electric field distribution in the trench corner area of the traditional 1.2 kV trench MOSFET and a trench MOSFET equipped with a buried p-type grid is shown at a drain bias of 600 V. The function of the extra grid is to screen off the electric field from the trench corners by taking up the voltage. A significant reduction of the electric field at the trench corner can be seen. The peak electric field in the oxide is reduced from 7.6 to 3.4 MV/cm in the example shown. The specific on-resistance of the structures is 1.0 and 1.1 $m\Omega\,cm^2$, respectively, for a pitch of 3 μm and grid spacing of about 1.2 μm. This type of device can be viewed as a high voltage JFET coupled with a low voltage control device. A MOSFET can easily be replaced by a low voltage JFET thus constituting a buried grid high voltage SIT device. In Fig. 13 the forward blocking characteristics and a cross-section of a 1.2 kV SIT device based on this principle is shown. The blocking gain of the device having a pitch and channel width of 12 and 1.8 μm, respectively, is about 30 and the specific on-resistance is about 10 $m\Omega\,cm^2$ with 2 V bias applied to the gate. The buried grid concept opens a number of other possibilities.

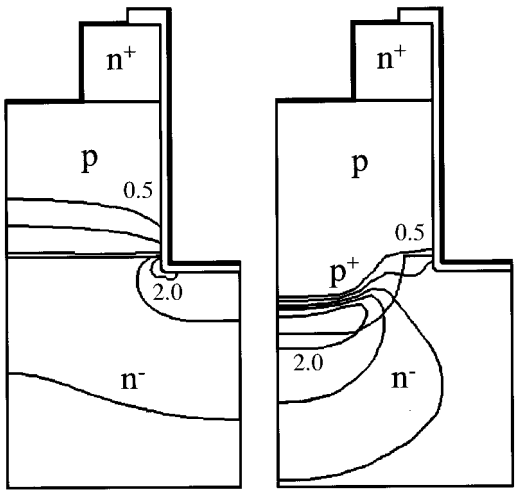

Fig. 12. The electric field distribution in the trench corner area of the standard trench MOSFET (left part)and the buried grid trench MOSFET (right part). The electric field lines are shown for 5×10^5, 1×10^6, 1.5×10^6, 1.75×10^6 and 2×10^6 V/cm

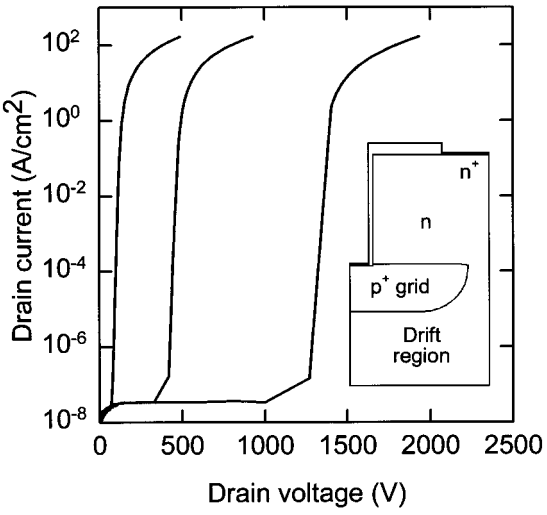

Fig. 13. The forward blocking characteristics with gate voltages −10, −20 and −40 V and the structure (half cell) of the 1.2 kV SIT with buried grid

7. Conclusions

Based on a fairly limited set of basic models predictions can be made with respect to the feasibility and attractiveness of different device concepts. In this context simulation is used as a guidance in choosing the most viable concepts for the development.

It is clearly seen from the simulations that the area of silicon carbide unipolar devices is greatly expanded compared to silicon. 4H-SiC MOSFETs represent an attractive choice from the point of view of total losses and on-state voltage up to 4.5 kV compared with the SiC IGBTs. At frequencies above 5 kHz the 4H-SiC MOSFETs have lower total losses compared to the IGBTs even at the design voltage of 25 kV. The on-state voltage of the 25 kV MOSFET is, however, about seven times higher than for the equivalent IGBT, at current densities in the range between 50 and 100 A/cm^2.

Based on the presented simulations and calculation of the total losses the area of bipolar SiC devices is predicted to be above 4.5 kV for IGBTs and above 2.5 kV for PiN rectifiers. The unipolar alternatives, MOSFETs and Schottky rectifiers, are predicted to dominate below those limits.

The gate reliability issues are considered to be a far more serious limitation of the SiC MOS-type devices with insulated gate, like MOSFETs and IGBTs, than the low channel mobility limitation. The development of practical MOSFETs in SiC requires further improvements in the oxide technologies or a development of an alternative gate dielectric.

The reliability problems are also fuelling the search for alternative solutions. New structures with reduced values of the electric field at the SiC and dielectric interface will be developed and alternative structures and concepts not requiring the dielectric will be explored. The buried grid structures presented in this article are an example of such endeavours.

Acknowledgements This work was funded jointly by ABB and the Swedish National Board for Industrial and Technical Development (NUTEK).

References

[1] P.A. Ivanov and V.E. Chelnokov, Semicond. Sci. Technol. **7**, 863 (1992).
[2] M. Bhatnagar and B.J. Baliga, IEEE Trans. Electron Devices **40**, 645 (1993).
[3] R. Helbig, Proc. 5th Internat. Symp. Power Semicond. Devices and ICs, Monterey (CA), May 1993, IEEE Eds. (p. 6).
[4] M. Bhatnagar and B.J. Baliga, Proc. 3th Internat. Symp. Power Semicond. Devices and ICs, Baltimore (MD), April 1991, IEEE Eds. (p. 176).
[5] H. Funaki, A. Nakagawa, and I. Omura, see [3] (p.212).
[6] M. Ruff, H. Mitlehner, and R. Helbig, IEEE Trans. Electron Devices **41**, 1040 (1994).
[7] B.J. Baliga, Microelectronic Engng. **28**, 177 (1995).
[8] N. Mohan, T.M. Undeland, and W.P. Robbins, Power Electronics: Converters, Applications and Design, Wiley, New York 1989.
[9] U. Lindefelt, J. Appl. Phys. **76**, 4164 (1994).
[10] U. Lindefelt, J. Appl. Phys. **75**, 942 (1994).
[11] O. Tornblad, U. Lindefelt, and B. Breitholtz, Solid State Electronics **39**, 1463 (1996).
[12] W.J. Schaffer, G.H. Negley, K.G. Irvine, and J.W. Palmour, Mater. Res. Soc. Symp. Proc. **339**, 595 (1994).
[13] L. Patrick and W.J. Choyke, Phys. Rev. B **2**, 2255 (1970).
[14] S. Ninomiya and S. Adachi, Japan. J. Appl. Phys. **33**, 2479 (1994).
[15] A.O. Konstantinov, Soviet Phys. – Semicond. **23**, 31 (1989).
[16] A.P. Dmitriev, A.O. Konstantinov, D.P. Litvin, and V.I. Sankin, Soviet Phys. – Semicond. **17**, 686 (1983).
[17] C. Persson and U. Lindefelt, to be published.
[18] G.L. Harris (Ed.), Properties of Silicon Carbide, INSPEC, The Institution of Electrical Engineers, London 1995.
[19] R. Dalven, J. Phys. Chem. Solids **26**, 439 (1965).
[20] W.J. Choyke and L. Patrick, Phys. Rev. **105**, 1721 (1957).
[21] A.O. Evwaraye, S.R. Smith, and W.C. Mitchel, Appl. Phys. Lett. **67**, 3319 (1995).
[22] S. Selberherr, in: Analysis and Simulation of Semiconductor Devices, Springer-Verlag, Wien 1984.
[23] U. Lindefelt, unpublished.
[24] C. Persson and U. Lindefelt, Phys. Rev. B **54**, 10257 (1996).
[25] D. Volm, B.K. Meyer, D.M. Hofmann, W.M. Chen, N.T. Son, C. Persson, U. Lindefelt, O. Kordina, E. Sörman, A.O. Konstantinov, B. Monemar, and E. Janzén, Phys. Rev. B **53**, 15409 (1996).
[26] M. Ikeda, H. Matsunami, and T. Tanaka, Phys. Rev. B **22**, 2842 (1980).
[27] W. Götz, A. Schöner, G. Pensl, W. Suttrop, W.J. Choyke, R. Stein, and S. Leibenzeder, J. Appl. Phys. **73**, 3332 (1993).
[28] J. Dziewior and W. Schmid, Appl. Phys. Lett. **31**, 346 (1977).
[29] M. Bakowski, Electron Technology **26**, 95 (1993).
[30] A. Porst, Proc. 6th Internat. Symp. Power Semicond. Devices and ICs, Davos (Switzerland), May/June 1994, Hartung-Garre Verlag, Konstanz (p. 163).
[31] H. Gruening and J. Voboril, Archiv für Elekrotechnik **72**, 69 (1989).
[32] J.Yamashita, H. Haruguchi, and H. Hagino, see [30] (p. 45).
[33] M. Bakowski and U. Gustafsson, Proc. 7th Symp. Power Semicond. Devices and ICs, Yokohama (Japan), May 1995, Inst. Electr. Eng. Japan (p. 354).
[34] H. Kabza, H.J. Schulze, Y. Gerstenmaier, F. Pfirsch, and K. Platzder, see [32] (p. 9).
[35] H.R. Zeller, see [32] (p. 339).
[36] A. Hallén, private communication.
[37] M. Bhatnagar, P.K. McLarty, and B.J. Baliga, IEEE Electron Device Lett. **13**, 501 (1992).
[38] K. Ueno, T. Urushidani, K. Hashimoto, and Y. Seki, see [33] (p. 107).
[39] T. Kimoto, T. Urushidani, S. Kobayashi, and H. Matsunami, IEEE Electron Device Lett. **14**, 548 (1993).
[40] A. Itoh, T. Kimoto, and H. Matsunami, Proc. 6th Silicon Carbide and Related Materials Conf., Inst. Phys. Ser. **142**, 689 (1995).

[41] D. Stephani, Abstracts 1st Europ. Conf. Silicon Carbide and Related Materials, Heraklion (Crete), October 1996 (p. 92).
[42] U. Gustafsson, M. Bakowski, and U. Lindefelt, see [40], Inst. Phys. Ser. **142**, 793 (1995).
[43] M. Bakowski, U. Gustafsson, and L.P. Ramberg, Proc. 24th Europ. Conf. Solid State Device Res., Edinburgh, September 1994, Editions Frontieres (p. 761).
[44] A.K. Agarwal, R.R. Siergiej, S. Seshadri, M.H. White, P.G. McMullin, A.A. Burk, L.B. Rowland, C.D. Brandt, and R.H. Hopkins, Proc. 8th Internat. Symp. Power Semicond. Devices and ICs, Maui (Hawaii) May 1996, IEEE Eds. (p. 119).
[45] J.W. Palmour, L.A. Lipkin, R. Singh, D.B. Slater, and A. Suvorov, see [41] (p. 52).
[46] J.W. Palmour, C.H. Carter, C.E. Eitzel, and K.J. Nordquist, Mater. Res. Soc. Symp. Proc. **339**, 133 (1994).
[47] L.A. Lipkin and J.W. Palmour, J. Electronic Mater. **25**, 909 (1996).
[48] B. Hornetz, H.J. Michel, and J. Halbritter, J. Vacuum Sci. Technol. A **13**, 767 (1995).
[49] V.V. Afanasev, A. Statesmans, M. Bassler, G. Pensl, M.J. Schulz, and C.I. Harris, Appl. Phys. Lett. **68**, 2141 (1996).
[50] S. Kobayashi, T. Kimoto, and H. Matsunami, Japan. J. Appl. Phys. **35**, 3331 (1996).
[51] M. Bakowski and U. Gustafsson, Proc. 26th Europ. Solid State Device Res. Conf., Bologna, September 1996, Editions Frontieres (p. 583).
[52] S.M. Sze, Physics of Semiconductor Devices, 2nd ed., Wiley, New York 1981 (p. 104).
[53] J.A. Edmond, D.G. Waltz, S. Brueckner, H.-S. Kong, J.W. Palmour, and C.H. Carter, Proc. 1st Internat. High Temp. Electronics Conf., Albuquerque (NMex), 1991 (p. 500).
[54] R.C. Clarke, A.K. Agarwal, R.R. Siergiej, C.D. Brandt, and A.W. Morse, 54th Ann. Device Res. Conf. Digest, Santa Barbara, June 1996, IEEE Eds. (p. 62).
[55] J.M. McGarrity, F.B. McLean, W.M. De Lancey, J. Palmour, C. Carter, J. Edmond, and R.E. Oakley, IEEE Trans. Nuclear Sci. **39**, 1974 (1992).
[56] P.A. Ivanov, Russian Phys. – Semicond. **28**, 662 (1994).
[57] C.E. Weitzel, J.W. Palmour, C.H. Carter, and K.J. Nordquist, IEEE Trans. Electron Devices **15**, 406 (1994).
[58] B.J. Baliga, see [40], Inst. Phys. Ser. **142**, 1 (1995).